Journal of Chemical Physics
March 2008 ; Volume 128 (11) : NIL_306-NIL_315
http://dx.doi.org/10.1063/1.2827490

The double Renner effect in the $\tilde{X}\ ^2A''$ and $\tilde{A}\ ^2A'$ electronic states of HO_2

Vladlen V. Melnikov[1], Tina Erica Odaka[3], Per Jensen[1,*] and Tsuneo Hirano[2]

[1] Department of Chemistry, Faculty of Mathematics and Natural Sciences, University of Wuppertal, D-42097 Wuppertal, Germany
[2] Department of Chemistry, Faculty of Science, Ochanomizu University, 2-1-1 Otsuka, Bunkyo-ku, Tokyo 112-8610, Japan
[3] IFREMER, Centre de Brest, BP 70, 29280 – Plouzané - France

*: Corresponding author : Per Jensen, email address : jensen@uni-wuppertal.de

Abstract:

A theoretical investigation of the $\tilde{X}\ ^2A''$ and $\tilde{A}\ ^2A'$ electronic states of the HO_2 radical is reported. Both electronic states have nonlinear equilibrium geometries and they correlate with a $^2\Pi$ state at linear geometries so that they exhibit the Renner effect. In highly excited bending states, there is tunneling between two equivalent minima (with geometries where the H nucleus is bound to one, or the other, of the two O nuclei), and the two linear geometries H–O–O and O–O–H become accessible to the molecule. Thus, HO_2 affords an example of the so-called double Renner effect. Three-dimensional potential energy surfaces for the $\tilde{X}\ ^2A''$ and $\tilde{A}\ ^2A'$ electronic states of HO_2 have been calculated *ab initio* and the global potential energy surfaces for the states have been constructed. These surfaces have been used, in conjunction with the computer program DR [Odaka et al., J. Mol. Structure **795**, 14 (2006); Odaka et al., J. Chem. Phys. **126**, 094301 (2007)], for calculating HO_2 rovibronic energies in the "double-Renner"-degenerate electronic states $\tilde{X}\ ^2A''$ and $\tilde{A}\ ^2A'$. The results of the *ab initio* calculations, the rovibronic energies obtained, and analyses of the wavefunctions for selected states are presented.

I. INTRODUCTION

The hydroperoxyl radical, HO_2, is of crucial importance in the chemistry of the Earth's atmosphere.[1] It is a key oxidizer, capable of reacting with volatile organic compounds and efficiently convert NO to NO_2 while regenerating OH.[2,3] It also plays a role in interstellar chemistry[4] and in combustion processes, for example as an intermediate in the reaction $H + O_2 \rightleftarrows HO + O$.[5–7] The first predictions of the properties of HO_2 were made by Walsh[8] in 1952. He obtained the ground electronic state to have a bent equilibrium geometry and the first excited electronic state to be very low in energy. These predictions were later confirmed by more detailed *ab initio* calculations.[9,10] At linear geometries, the electronic ground state is $^2\Pi$, and this state splits into the non-degenerate $\widetilde{X}\ ^2A''$ and $\widetilde{A}\ ^2A'$ states when the molecule bends. Both of these states have strongly bent equilibrium geometries. Since they correlate with a $^2\Pi$ state at linearity, the $\widetilde{X}\ ^2A''$ and $\widetilde{A}\ ^2A'$ states exhibit the Renner effect[11] (see also Refs. 12, 13 and references therein).

The $\widetilde{A}-\widetilde{X}$ electronic band system of HO_2 in the gas phase was studied experimentally in 1974, both in emission and absorption,[14,15] and it was realized that forbidden $\Delta K_a = 0$ transitions are present. Tuckett *et al.*[16] suggested that these transitions result from Renner interaction. Several spectroscopic studies followed.[16–22] Fairly recently, Fink and Ramsay[22] carried out a high-resolution re-investigation of the $\widetilde{X}/\widetilde{A}(v_1, v_2, v_3) = \widetilde{A}(0,0,0) \rightarrow \widetilde{X}(0,0,0)$ band. They also observed forbidden $\Delta K_a = 0$ transitions and concluded that these are magnetic dipole transitions. The electric dipole transition moment for the electronic transition was found to be very small.

To confirm the analysis by Fink and Ramsay,[22] Osmann *et al.*[23] calculated *ab initio* the potential energy, transition electric dipole and transition magnetic dipole surfaces of the $\widetilde{X}\ ^2A''-\widetilde{A}\ ^2A'$ system and simulated the $\widetilde{A}\ ^2A' \rightarrow \widetilde{X}\ ^2A''$ emission spectrum with the program RENNER.[24–26] Later, Jensen *et al.*[27] calculated more points on the potential energy surfaces, using the *ab initio* method of Ref. 23, to cover a wider range of bending geometries. They adjusted the shapes of the surfaces in a least squares refinement to the energies of rovibronic states involving both electronic states. Their results provide an accurate representation of the surfaces in this energy region and confirmed the conclusions by Fink and Ramsay,[22] in particular the assignment of the forbidden $\Delta K_a = 0$ transitions as magnetic dipole transitions. Also, Jensen *et al.*[27] explained a perturbation observed by Fink and Ramsay[22] in the

$\widetilde{A}(0,0,0) \rightarrow \widetilde{X}(0,0,0)$ band for states with $J \approx 51/2$. The theoretical identification of the perturbing state has been confirmed in a very recent re-analysis of the experimental data.[28] In another recent experimental study[29] of $\widetilde{X}\ ^2A''$ HO_2, the $2\nu_1$ band has been investigated by diode laser spectroscopy.

Compared to that of an 'ordinary' triatomic molecule with an isolated electronic ground state, H_2O say, the theoretical description of the rotation and vibration in the electronic ground state $\widetilde{X}\ ^2A''$ of HO_2 is subject to two complications. The first one is the presence of the Renner effect which causes the $\widetilde{X}\ ^2A''$ state to be degenerate with the first excited state, $\widetilde{A}\ ^2A'$, at linear geometries. In consequence, the Born-Oppenheimer approximation (see, for example, Ref. 30 and the references therein) breaks down and the $\widetilde{X}\ ^2A''$ and $\widetilde{A}\ ^2A'$ states must be treated together. The second complication is that in both the $\widetilde{X}\ ^2A''$ and $\widetilde{A}\ ^2A'$ electronic states, HO_2 has two *versions*, i.e., non-superposable equilibrium structures that differ only in the numbering of identical nuclei.[31] The two versions have the H nucleus bound to one, or the other, of the two O nuclei, at the strongly bent equilibrium geometries of the $\widetilde{X}\ ^2A''$ and $\widetilde{A}\ ^2A'$ states. In highly excited bending states there is tunneling between two equivalent minima corresponding to the two versions, and the two linear geometries H-O-O and O-O-H, each one associated with a doubly degenerate, $^2\Pi$ electronic state, become accessible to the molecule. Thus, HO_2 affords an example of the so-called double Renner effect.[32–34]

To the best of our knowledge, the first theoretical investigation of the double Renner effect for $\widetilde{X}\ ^2A''/\widetilde{A}\ ^2A'$ HO_2 was described fairly recently by Odaka,[32] who presented preliminary results only. In the present work, we have calculated, by *ab initio* methods, new potential energy surfaces for the $\widetilde{X}\ ^2A''$ and $\widetilde{A}\ ^2A'$ states of HO_2, improving the coverage of configuration space relative to the *ab initio* data set (from Refs. 23,27) available to Odaka,[32] in particular in the region near the tops of the potential energy barriers separating the two equivalent minima in the two electronic states. In this manner, we obtain more accurate rovibronic energies and a deeper insight into the effects of Renner degeneracy combined with tunneling between two equivalent minima on the two potential energy surfaces involved.

We have calculated three-dimensional potential energy surfaces for the $\widetilde{X}\ ^2A''$ and $\widetilde{A}\ ^2A'$ electronic states of HO_2 *ab initio* at the full-valence multi-reference single and double excitation configuration (MR-SDCI) + Davidson correction Q level of theory including core-valence correlations, based on the two-state (i.e., one A' and one A'' state) averaged, no-core, full-

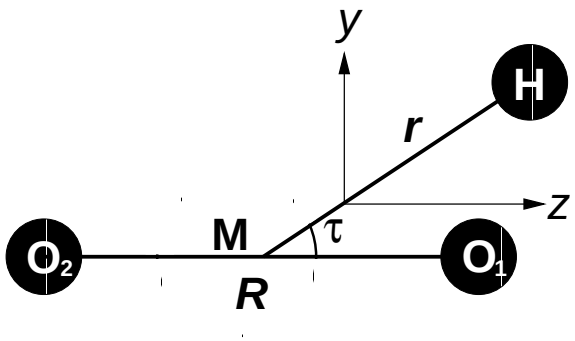

FIG. 1: The Jacobi coordinates, and the molecule-fixed axis system xyz, for HO_2. The O nuclei are labeled 1 and 2, respectively, as indicated, and the proton is labeled 3. M is the center of mass of the OO moiety. The O-O internuclear distance is called R, r is the M-H distance, and τ = $\angle$(O_1-M-H) where O_1 is the oxygen nucleus labeled 1. The xyz axis system has origin in the nuclear center of mass. The z axis is parallel to the O-O bond, and the x axis points into the plane of the page so that the xyz axis system is right-handed.

valence CASSCF orbitals, with a Dunning cc-pVQZ basis set for H and an aug-cc-pCVQZ basis set for O. From the results of the *ab initio* calculations, global potential energy surfaces for the $\widetilde{X}\ ^2A''$ and $\widetilde{A}\ ^2A'$ electronic states have been constructed. These surfaces have been used, in conjunction with the newly developed computer program DR,[32–34] for calculating HO_2 rovibronic energies in the double-Renner-degenerate electronic states. The rovibronic wavefunctions for selected states have been analyzed.

II. THEORY

The theoretical model used in the present work is described in detail in Ref. 33 and summarized in Ref. 34. The reader is referred to these references and to Ref. 32 which gives extensive details, such as explicit expressions for many matrix elements. The vibrational motion of HO_2 is described by Jacobi coordinates (r, R, τ) which are defined, together with the chosen molecule-fixed axis system xyz, in Fig. 1. The theoretical model is implemented in the DR program which determines the eigenvalues and eigenfunctions of the rovibronic Hamiltonian $\hat{H}_{\rm DR}$ in a standard variational calculation: The matrix representation of $\hat{H}_{\rm DR}$ is constructed in terms of suitable basis functions[32,33] and diagonalized numerically. In the DR calculations for $\widetilde{A}\ ^2\Pi$ MgNC/MgCN reported in Refs. 32,33, and in the HO_2 calculations of

the present work, the diagonalizations are carried out by means of the LAPACK[35] driver DSYEVX, whereas Ref. 34 reported the implementation of a newly developed, highly efficient matrix diagonalization routine in the DR program and the application of the improved program to the calculation of high-J energies for $\widetilde{A}\ ^2\Pi$ MgNC/MgCN.

For HO_2, the eigenstates of $\hat{H}_{\rm DR}$ are labeled by the good quantum numbers J, M_J, S, and $\Gamma_{\rm rve}$, where the quantum number J pertains to the operator $\hat{\boldsymbol{J}}^2 = (\hat{\boldsymbol{N}} + \hat{\boldsymbol{S}})^2$ with $\hat{\boldsymbol{N}}$ as the total orbital angular momentum and $\hat{\boldsymbol{S}}$ as the total electron spin; $M_J\,\hbar$ is the projection of $\hat{\boldsymbol{J}}$ on the space-fixed Z axis (see, for example, Ref. 12); S is associated with $\hat{\boldsymbol{S}}^2$ and $\Gamma_{\rm rve}$ is the symmetry of the eigenstate in the molecular symmetry group[12] of HO_2

$$\boldsymbol{C}_{2\rm v}({\rm M}) = \{E, (12), E^*, (12)^*\}\,. \tag{1}$$

Here, E is the identity operation, (12) is the transposition[12] (interchange) of the two O nuclei (which we label 1 and 2 as shown in Fig. 1), the inversion operation[12] E^* inverts all nuclei and electrons in the molecular center of mass, and $(12)^* = (12)\,E^*$. The operations (12) and $(12)^*$ are feasible[12] because, as discussed above, we take into account the tunneling between the two versions of HO_2. The character table of $\boldsymbol{C}_{2\rm v}({\rm M})$ is given in Table A-5 of Ref. 12; the four possible irreducible representations are $\Gamma_{\rm rve} = A_1$, A_2, B_1, or B_2.

In Refs. 32–34 we described DR calculations for $\widetilde{A}\ ^2\Pi$ MgNC/MgCN with the molecular symmetry group $\boldsymbol{C}_{\rm s}({\rm M}) = \{E, E^*\}$. For this molecule, all vibrational basis functions [which depend on the Jacobi coordinates (r, R, τ) defined in Fig. 1] are totally symmetric in the molecular symmetry group because the Jacobi coordinates are invariant under E^*. For HO_2, the Jacobi coordinates are also invariant under E^*. However, under (12) and $(12)^*$ we have

$$(12)\,(r, R, \tau) = (12)^*\,(r, R, \tau) = (r, R, \pi - \tau). \tag{2}$$

Thus, vibrational basis functions for HO_2 can have A_1 or B_2 symmetry in $\boldsymbol{C}_{2\rm v}({\rm M})$. Functions with A_1 symmetry satisfy $\psi_{\rm vib}(r, R, \pi - \tau) = \psi_{\rm vib}(r, R, \tau)$, and functions with B_2 symmetry satisfy $\psi_{\rm vib}(r, R, \pi - \tau) = -\psi_{\rm vib}(r, R, \tau)$.

III. POTENTIAL ENERGY SURFACES

A. Ab initio calculations

We have used the MOLPRO[36] suite of quantum chemistry programs for carrying out *ab initio* calculations to determine the potential energy surfaces (PESs) for the $\widetilde{X}\ ^2A''$ and $\widetilde{A}\ ^2A'$ states of HO_2. The corresponding dipole moment and transition moment surfaces were also calculated. The basis set employed for the hydrogen atom was the Dunning[37] correlation-consistent valence quadruple-zeta basis set (cc-pVQZ),$(6s,3p,2d,1f)/[4s,3p,2d,1f]$, and that for the oxygen atom was the Dunning and coworkers[37–39] augmented correlation-consistent polarized core-valence valence quadruple-zeta basis set (aug-cc-pCVQZ),$(16s,10p,6d,4f,2g)/[9s,8p,6d,4f,2g]$.

Starting from restricted Hartee-Fock (RHF) orbitals for the $\widetilde{X}\ ^2A''$ state of HO_2 as the initial guess, multi-configuration self-consistent field (MCSCF) molecular orbitals (MOs), averaged over the $\widetilde{X}\ ^2A''$ and $\widetilde{A}\ ^2A'$ states, have been fully optimized for the full valence active space (13 electrons in 9 orbitals) with constraint of double occupancy in the oxygen $1s$ orbitals. Based on these state-averaged MCSCF natural orbitals (NOs), internally contracted MR-SDCI (multi-reference single and double excitation configuration interaction) calculations, each for the $\widetilde{X}\ ^2A''$ and $\widetilde{A}\ ^2A'$ states, were carried out for the full valence active space (13 electrons in 9 orbitals), where core-valence and core-core correlations were also included by single and double excitations from 1- and 2-a' orbitals (primarily originating in oxygen $1s$-orbitals) in each configuration state function. Dynamical electron correlation due to quadruple excitations was subsequently recovered by the Davidson correction[40] $+Q$. Thus, our method will be denoted as core-valence MR-SDCI+Q/[cc-pVQZ (H), aug-cc-pCVQZ (O)]. The PESs have been calculated with this method under $\boldsymbol{C}_{\rm s}$ symmetry, the nuclear geometries being specified by the Jacobi coordinates defined in Fig. 1.

The actual procedure for carrying out the *ab initio* calculations is as follows. At the MR-SDCI+Q level, we first located two transition states (TSs), one at $\tau = 0$ (linear structure) and the other at $\tau = 90^\circ$ (T-shaped transition structure for the isomerization between the H-O-O and O-O-H structures) under $\boldsymbol{C}_{2\rm v}$ symmetry constraint, and then traced the minimum energy path (MEP) from each of the TS structures down to each equilibrium structure on the A'' and A' PESs under $\boldsymbol{C}_{\rm s}$ symmetry. We varied τ in steps of 10° to 15° in the interval

TABLE I: Geometries of the stationary points on the potential energy surfaces for the $\widetilde{X}\ ^2A''$ and $\widetilde{A}\ ^2A'$ electronic states of HO_2, derived from the analytical PESs based on the core-valence MR-SDCI+Q/[cc-pVQZ (H), aug-cc-pCVQZ (O)] *ab initio* data. See Fig. 1 for the definition of the coordinates (r, R, τ).

	r/Å	R/Å	τ	r(H-O)/Å	∠(H-O-O)
$\widetilde{X}\ ^2A''$ equilibrium geometry	1.3065	1.3311	45.97°	0.9702	104.48°
$\widetilde{A}\ ^2A'$ equilibrium geometry	1.3047	1.3986	46.54°	0.9676	101.81°
Maximum at linearity ($^2\Pi$) on the MEP	1.6060	1.3276	0°/180°	0.9422	180°
Transition state for isomerization ($\widetilde{X}\ ^2A''$)	0.9172	1.4303	90°	1.1630	52.06°
Transition state for isomerization ($\widetilde{A}\ ^2A'$)	0.9489	1.4275	90°	1.1874	53.05°

$0° < \tau < 90°$ and, for each τ-value considered, we calculated two-state averaged CASSCF NOs for various combinations of the r and R distances perpendicular to the MEP, using the CASSCF NOs optimized for the corresponding point on the MEP having the given τ as the initial-guess orbitals for the state-averaged (SA) CASSCF calculation. Then, based on the SA-CASSCF NOs thus determined, we carried out MR-SDCI+Q calculations. Considering the symmetry situation we mapped these energies onto the entire configuration space with $0° < \tau < 180°$. The energies at $\tau = 0°$, 90°, and 180° were determined by interpolation. Thus, actual calculations of the $\widetilde{X}\ ^2A''$ and $\widetilde{A}\ ^2A'$ state electronic energies have been done for 384 geometries with $0° < \tau < 90°$.

The geometries, at which *ab initio* calculations were carried out, were selected such that their energies are less than 25000 cm^{-1} above the global minimum. Additional points were calculated to improve the coverage of geometries with energies below 6000 cm^{-1} and geometries near the global minima and the MEP. Thus, a large fraction of the calculated points are located in the corresponding regions of configuration space.

The energy variation with τ along the calculated MEPs for the $\widetilde{X}\ ^2A''$ and $\widetilde{A}\ ^2A'$ states, respectively, are shown in Fig. 2. The energy at linearity (i.e., at $\tau = 0°$ and 180°) is 20644.1 cm^{-1} above the equilibrium energy of the $\widetilde{X}\ ^2A''$ state and 13478.6 cm^{-1} above that of the $\widetilde{A}\ ^2A'$ state and the barriers at $\tau = 90°$, corresponding to T-shaped geometry, are 13449.6 and 11810.9 cm^{-1} in the $\widetilde{X}\ ^2A''$ and the $\widetilde{A}\ ^2A'$ states. The energy difference between the global minima of two electronic states is 7165.5 cm^{-1}. The geometries for these stationary points, derived from the fitted analytical PESs (see Section III B), are given in Table I.

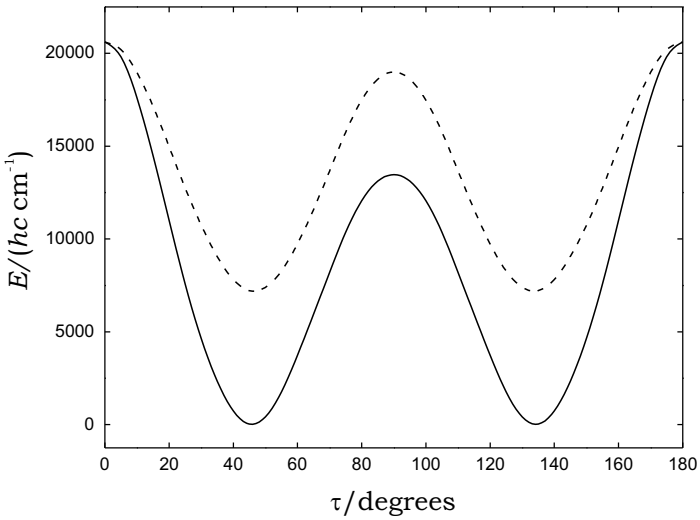

FIG. 2: The bending minimum energy paths for HO_2. The solid curve corresponds to the $\widetilde{X}\ ^2A''$ electronic state and the dashed curve to the $\widetilde{A}\ ^2A'$ state.

B. Analytical potential energy surfaces

We now fit analytical, parameterized representations of the potential energy functions of $\widetilde{X}\ ^2A''$ and $\widetilde{A}\ ^2A'$ HO_2 through the calculated *ab initio* points; the optimized parameter values are used as input for the DR program. From the analytical potential energy functions, the DR program can generate the electronic energies at any nuclear geometry; this is required for carrying out the numerical integrations producing the matrix elements of $\hat{H}_{\rm DR}$. We choose the following analytical functions to represent the potential energy surfaces:

$$V^{\sigma}(r,R,\tau) = \sum_{i,j,k} F^{\sigma}_{ijk}\ (\xi_r)^i\,(\xi_R)^j\,(\xi_\tau)^k, \tag{3}$$

where

$$\xi_r = 1 - \exp[-\beta_r(r - r^{\sigma}_{\rm e})], \tag{4}$$

$$\xi_R = 1 - \exp[-\beta_R(R - R^{\sigma}_{\rm e})], \tag{5}$$

$$\xi_\tau = 1 - \cos 2\tau. \tag{6}$$

In these expressions, σ denotes the electronic state with $\sigma = -$ and $+$ for the $\widetilde{X}\ ^2A''$ and $\widetilde{A}\ ^2A'$ states, respectively. The quantities $r^{\sigma}_{\rm e}$ and $R^{\sigma}_{\rm e}$ depend on τ and are expressed as the series

$$r^{\sigma}_{\rm e} = \sum_k f^{r,\sigma}_k\ (\xi_\tau)^k, \quad R^{\sigma}_{\rm e} = \sum_k f^{R,\sigma}_k\ (\xi_\tau)^k\,. \tag{7}$$

The values of the parameters $f_i^{r,\sigma}$ and $f_i^{R,\sigma}$ were determined by fitting the analytical functions in Eq. (7) through the values of R and r determined along the MEP as τ is varied. That is, for a given value of τ, $(r_e^\sigma, R_e^\sigma, \tau)$ defines the geometry of the local potential energy minimum for the electronic state σ.

Since we are expanding the PESs in terms of the variable ξ_τ in Eq. (6), we trivially have that (12) $V^\sigma(r, R, \tau) = V^\sigma(r, R, \pi - \tau) = V^\sigma(r, R, \tau)$ as required by symmetry.[12] For linear geometries ($\tau = 0°$ and 180°) we have $\xi_\tau = 0$. By setting $F_{ij0}^- = F_{ij0}^+$ in Eq. (3) we achieve that the degeneracy of the two potential energy surfaces at linear geometries is correctly described. Since the F_{ij0}^- parameters are common to the two surfaces, we determine the values of the potential energy parameters F_{ijk}^σ and the exponents β_r and β_R in simultaneous fittings to the *ab initio* points for both electronic states involved.

The expansions of Eq. (3) have proved adequate for fitting the *ab initio* data for the $\widetilde{X}\ ^2A''$ and $\widetilde{A}\ ^2A'$ states of HO_2. However, when we wish to describe not only the PESs in the vicinity of the potential energy minima, as done in Refs. 23 and 27, but also the detailed shapes of the barriers to linearity and the barrier to H-O-O $\leftrightarrow$ O-O-H tunneling, we find that terms of very high order must be included in the series expansions of Eq. (3). To obtain reliable values for the corresponding high-order expansion coefficients F_{ijk}^σ, we would require an extremely extensive set of *ab initio* points which, with the computer resources available to us, we cannot calculate in practice. Consequently, in accordance with our strategy for selecting the nuclear geometries for the *ab initio* points, we have chosen a fitting strategy which favours the regions of configuration space near the minima and near the MEPs while still producing physically sound PESs of an acceptable accuracy in other regions. In particular, we give lower weights to *ab initio* points at high energy since the accuracy of the *ab initio* calculation at such points, where the molecule is strongly displaced from its equilibrium geometry, is known to be less than that of points near the minima.

According to our fitting strategy, the *ab initio* points available for each of the two electronic states are divided into two subsets. The first subset contains all points with energies below a chosen value, $E_{\max}^\sigma$ say, measured relative to the energy of the global minimum, and the points in the immediate vicinity of the MEP. The second subset consists of the remaining data points. Thus, the points in the first subset define the PES in the regions of configuration space sampled by the wavefunctions of the states that have been characterized experimentally. By adjusting the weights of the points in the second subset of data, and

the value of $E^{\sigma}_{\rm max}$, we can achieve a satisfactory reproduction of the energy values of the first subset while - since the points in the second subset are not discarded - we obtain PESs with physically correct shapes also in the regions of configuration space corresponding to the second subset. Owing to the fact that we are describing with good accuracy the regions of the MEPs, we expect satsfactory results for highly excited bending states and, therefore, a correct description of the double Renner effect and the H-O-O $\leftrightarrow$ O-O-H tunneling.

The potential energy parameter values resulting from the final fitting are listed in Table II. The values of $E^{\sigma}_{\rm max}$ were taken as 6000 cm^{-1} for the $\widetilde{X}\ ^2A''$ state and 12300 cm^{-1} for the $\widetilde{A}\ ^2A'$ state. The final fit included 339 $\widetilde{X}\ ^2A''$-state data points and 327 $\widetilde{A}\ ^2A'$-state data points, some of the 384 data points initially available for each surface having been discarded since they correspond to extremely high energies. The corresponding weighted standard deviations are 12 and 10 cm^{-1}, respectively. The root-mean-square (rms) deviations for the first subset of data are 17 and 13 cm^{-1}, respectively, for $\widetilde{X}\ ^2A''$ and $\widetilde{A}\ ^2A'$ states, and the corresponding rms deviation for all data points are 270 and 250 cm^{-1}. Thus the global PESs have correct shapes and reasonable accuracy so that they can be used for qualitative studies of highly excited vibrational states.

IV. ROVIBRONIC ENERGIES

A. Computational details

With the DR[32–34] program, we have computed rovibronic energies and wavefunctions for $\widetilde{X}\ ^2A''$ and $\widetilde{A}\ ^2A'$ $H^{16}O_2$. As input for this calculation, we used the values of the parameters in the functions of Eqs. (3)-(7); these parameter values were obtained by fitting to the *ab initio* data as described in the preceding section.

The size of the vibrational basis set was determined by the parameter values (see Ref. 33) $(v_2^a)^{(\max)} = 23$, $(v_2^b)^{(\max)} = 15$, $N_R^{(\max)} = 15$, and $N_r^{(\max)} = 7$. In calculating integrals over τ, we have employed 4000 integration points for the Numerov-Cooley integrations, and 120 integration points for the Gauss-Laguerre integrations.

For the stretching basis functions $|N_R, \Gamma_R\rangle$ and $|N_r, \Gamma_r\rangle$ (see Ref. 33) we have used the parameter values $R_{\rm e} = 2.539041\ a_0$ and $r_{\rm e} = 2.484028\ a_0$, $D_{\rm e}^{(R)} = 0.175\ E_{\rm h}$, $D_{\rm e}^{(r)} = 15\ E_{\rm h}$, $h\,c\,\omega_{\rm e}^{(R)} = 0.004\ E_{\rm h}$, and $h\,c\,\omega_{\rm e}^{(r)} = 0.0125\ E_{\rm h}$. The number of integration points for Gauss-

TABLE II: The potential energy surface parameters for the $\widetilde{X}^2A''$ and $\widetilde{A}^2A'$ electronic states of HO_2, obtained by fitting to the *ab initio* data.

i	j	k	$F_{ijk}^{(-)}/\mathrm{cm}^{-1}$	$F_{ijk}^{(+)}/\mathrm{cm}^{-1}$	i	j	k	$F_{ijk}^{(-)}/\mathrm{cm}^{-1}$	$F_{ijk}^{(+)}/\mathrm{cm}^{-1}$
0	0	0	21206.48113145	21206.48113145	2	0	2	211649.64011518	41788.60551767
0	0	1	-59459.18302920	-35026.96131759	2	0	3	-228768.32950999	-38544.38529305
0	0	2	85855.52252558	45558.18176458	2	0	4	72371.62881977	19299.64435247
0	0	3	-94051.77609981	-51226.63452353	2	1	0	-367380.83606892	-367380.83606892
0	0	4	66769.76385630	39511.65394772	2	1	1	562480.78072702	641989.41256431
0	0	5	-23418.32245940	-15082.22586525	2	1	2	-280601.55811472	-344328.23204363
0	0	6	3136.63361043	2279.57755816	2	1	3	44547.94845415	57706.40222997
0	1	0	1937.15853020	1937.15853020	2	2	0	119997.17740321	119997.17740321
0	1	1	-26831.77879725	-15538.52779630	2	2	1	-419552.49119302	-420620.01638522
0	1	2	143993.16434417	93984.25692585	2	2	2	172680.54692549	187300.24068235
0	1	3	-229025.95173558	-162417.82990095	3	0	0	-34134.65591864	-34134.65591864
0	1	4	138873.43686970	105139.21406030	3	0	1	-406347.10510604	-403274.08034957
0	1	5	-28527.40897826	-22787.95235211	3	0	2	357358.16041934	422322.22831898
0	2	0	93301.91281253	93301.91281253	3	0	3	-81858.12717462	-119113.20399838
0	2	1	-121101.07003965	-47012.39783079	3	1	0	-38481.38832433	-38481.38832433
0	2	2	191012.40528087	57613.96903909	3	1	1	270782.45735030	206244.16017026
0	2	3	-129619.93498473	-49796.85586540	3	1	2	-138281.29375835	-104408.89942642
0	2	4	29541.85670368	12739.51896704	4	0	0	-209017.97799512	-209017.97799512
0	3	0	-76397.11449462	-76397.11449462	4	0	1	404062.31629245	393208.55685193
0	3	1	84287.58472590	132585.88551437	4	0	2	-167493.64422687	-146964.65147580
0	3	2	-23257.22298714	-80977.76241407					
0	3	3	736.06454530	17900.39091859		k		$f_k^{R,(-)}/\text{Å}$	$f_k^{R,(+)}/\text{Å}$
0	4	0	-25986.95332542	-25986.95332542					
0	4	1	45614.44682279	20286.51395863		0		1.31765641	1.31765641
0	4	2	-26834.64497559	-1916.37979036		1		-0.00743986	0.06478911
1	0	0	-4901.34371741	-4901.34371741		2		0.19913595	0.02615624
1	0	1	37919.92156565	5756.27543673		3		-0.91724319	-0.31436057
1	0	2	-197429.14954232	-86425.03536019		4		1.29731165	0.58554018
1	0	3	286810.84998363	162426.79829496		5		-0.68266057	-0.35673168
1	0	4	-147641.03139948	-95807.70958980		6		0.12116049	0.06948613
1	0	5	24572.53012016	17968.99540680					
1	1	0	-150625.82906308	-150625.82906308		k		$f_k^{r,(-)}/\text{Å}$	$f_k^{r,(+)}/\text{Å}$
1	1	1	267647.77244035	128476.13233165					
1	1	2	-236642.00314947	32900.90843857		0		1.60720702	1.60720702
1	1	3	128000.65115221	-48706.34858305		1		-0.12335863	-0.13944872
1	1	4	-26281.37181955	12052.38337157		2		-0.65289033	-0.56475817
1	2	0	316505.73443545	316505.73443545		3		1.36497455	1.20887929
1	2	1	-404318.88055143	-517601.40763006		4		-1.49587995	-1.36894866
1	2	2	131759.16520604	247485.09134230		5		0.76337930	0.72041450
1	2	3	-10818.40549357	-41839.87935608		6		-0.14433651	-0.13970290
1	3	0	-21091.50420203	-21091.50420203					
1	3	1	181257.49180234	190716.98433218					
1	3	2	-88584.85435677	-103898.85148800				$\beta_1 = 1.03$ Å^{-1}	$\beta_2 = 1.53$ Å^{-1}
2	0	0	225793.14584855	225793.14584855					
2	0	1	-133918.44496176	-138674.35038837					

Laguerre integration over the R and r coordinates were 15 and 35, respectively. The spin-orbit interaction constant for HO_2 was set to -160.1 cm^{-1} (Ref. 27). The threshold limit energy constant for K-block contraction,[32–34] E_{cont}, is taken to be 18000 cm^{-1}. All program parameters were adjusted to get the best fit to the *ab initio* PESs and MEPs and, at the same time, to achieve satisfactory convergence for the computed rovibronic energy values.

B. Results

The calculated rovibronic energy levels with $N_{K_aK_c} = 0_{00}$ (and $J = 1/2$) are listed in Table III.

Following Refs. 32–34, we analyze the wavefunctions of selected states by calculating probability distributions $f_1(\tau)$ and $f_2(r, \tau)$. The probability density function $f_1(\tau)$ [Eq. (37) of Ref. 33] is defined such that the differential probability dp_1 of finding the molecule with the bending coordinate in the infinitesimal interval between τ and $\tau + d\tau$ is given as

$$dp_1 = f_1(\tau)\, d\tau. \tag{8}$$

This function can be expressed as

$$f_1(\tau) = f_-(\tau) + f_+(\tau) \tag{9}$$

where $f_\sigma(\tau)\, d\tau$, $\sigma = -$ $(+)$ for the $\widetilde{X}\ ^2A''$ $(\widetilde{A}\ ^2A')$ state, is the differential probability of finding the molecule in the Born-Oppenheimer electronic state $\psi_{\rm e}^{(\sigma)}$ (i.e., $\psi_e^{(-)}$ for the $\widetilde{X}\ ^2A''$ state and $\psi_e^{(+)}$ for the $\widetilde{A}\ ^2A'$ state) with its bending coordinate between τ and $\tau + d\tau$. The functions $f_-(\tau)$ and $f_+(\tau)$ measure the extent of the mixing of the two electronic states $\psi_e^{(-)}$ and $\psi_e^{(+)}$ in the total rovibronic wavefunction at a given value of τ.

The over-all probability of finding the molecule in the Born-Oppenheimer electronic state $\psi_{\rm e}^{(\sigma)}$, $\sigma = -$ or $+$, is

$$P_\sigma = \int_0^\pi f_\sigma(\tau)\, d\tau \tag{10}$$

with $P_- + P_+ = 1$.

The probability density function $f_2(r, \tau)$ is given by Eq. (41) of Ref. 33. It is defined such that

$$dp_2 = f_2(r, \tau)\, dr\, d\tau \tag{11}$$

is the differential probability of finding the molecule with the bending coordinate in the infinitesimal interval between τ and $\tau + d\tau$ and the M-H distance (Fig. 1) in the interval between r and $r + dr$.

In the set of calculated rovibronic energy levels for HO_2 we can readily identify pairs of states resulting from H-O-O $\leftrightarrow$ O-O-H tunneling. In Table III, we give the rovibronic symmetries $\Gamma''_{\rm rve}/\Gamma'_{\rm rve}$ of both partner states in such pairs (for example as A_1/B_2 when the two partner states span the $\boldsymbol{C}_{2\rm v}$(M) representation[12] $A_1 \oplus B_2$). Here, $\Gamma''_{\rm rve}$ is the rovibronic

symmetry of the lower partner state with term value E given in the table, while $\Gamma'_{\rm rve}$ is the rovibronic symmetry of the upper partner state with term value $E + \Delta$, where the *tunneling splitting* Δ is also given in the table. In low-lying states, the tunneling is negligible, the partner states are effectively doubly degenerate, and $\Delta = 0$. In the table, we also list the value of P_+ for the lowest-energy partner state of each state pair; P_- can be obtained as $1 - P_+$.

In Table III, we compare the computed energies for the lowest rovibronic states with values obtained in the calculation by Jensen *et al.*[27] These authors correctly described the Renner effect by means of the program RENNER[24–26] but neglected the H-O-O $\leftrightarrow$ O-O-H tunneling. They used potential energy functions optimized in fittings to the experimentally available vibronic energies, and so their theoretical energy values are very close to the available experimental counterparts. The agreement between the DR energy values of the present work and the RENNER values from Ref. 27 is rather satisfactory and in keeping with the accuracy of the *ab initio* calculations. For the fundamental vibrational energies in the $\widetilde{X}\ ^2A''$ state, the differences are about 3 cm^{-1} for ν_3, 9 cm^{-1} for ν_2, and 19 cm^{-1} for ν_1. We conclude that the accuracy of the present calculations is satisfactory for the purpose of the present work: it is possible to make realistic investigations of the double Renner effect with the calculated potential energy surfaces. We note that, as mentioned above, the RENNER results are very close to the available experimental energy values, and so the purely *ab initio* results of the present work reproduce the experimental results well.

Figure 3 shows probability density functions $f_2(r, \tau)$ for the selected states indicated by (a)-(d) in Table III. The $f_2(r, \tau)$-function for the $\widetilde{X}(0, 0, 0)$, $J = 1/2$ state (marked (a) in Table III) is shown in Fig. 3(a). As expected, in this state (which originates completely in the $\widetilde{X}\ ^2A''$ electronic state) the probability density is localized near the two equilibrium geometries of the $\widetilde{X}\ ^2A''$ state, the one version having $(r_{\rm eq}, R_{\rm eq}, \tau_{\rm eq}) = (1.3065$ Å, 1.3311 Å, $45.9703°)$ and the other version having the same values of $R_{\rm eq}$ and $r_{\rm eq}$ but $\tau_{\rm eq}^{(2)} = \pi - \tau_{\rm eq}$. In general, the $\boldsymbol{C}_{2\rm v}$(M)-symmetry of HO_2 requires that $f_2(r, \tau) = f_2(r, \pi - \tau)$ as seen in the figure. The probability density function of the $\widetilde{A}(0, 0, 0)$, $J = 1/2$ state, calculated 7033.68 cm^{-1} above the $\widetilde{X}(0, 0, 0)$, $J = 1/2$ state and originating entirely in the $\widetilde{A}\ ^2A'$ electronic state, is very similar to that in Fig. 3(a) since the equilibrium geometries of the $\widetilde{X}\ ^2A''$ and $\widetilde{A}\ ^2A'$ states are very close. The $\widetilde{A}\ ^2A'$-state equilibrium geometry has $(r_{\rm eq}, R_{\rm eq}, \tau_{\rm eq})$ (1.3047 Å, 1.3986 Å, $46.5443°$).

TABLE III: Calculated term values E/hc (in cm^{-1}) for the $J = 1/2$, $N_{K_aK_c} = 0_{00}$ levels of $\widetilde{X}\ ^2A''$ and $\widetilde{A}\ ^2A'$ HO_2 up to 12750 cm^{-1} above the vibronic ground state. Probabilities P_+ of finding the molecule in the $\widetilde{A}\ ^2A'$ state, tunneling splittings Δ (in cm^{-1}) and rovibrational symmetry labels $\Gamma_{\rm rve}$ are given (see text). For the states indicated by (a)-(d), probability density functions $f_2(r,\tau)$ (see text) are shown in Fig. 3.

State	E	Ref. 27	$\Gamma_{\rm rve}$	P_+	Δ	E	$\Gamma_{\rm rve}$	P_+	Δ	E	$\Gamma_{\rm rve}$	P_+	Δ
$\widetilde{X}\ ^2A''(0,0,0)$	0.00[a]	0.0	A_2/B_1	0.00	0.00	8603.44	B_1/A_2	0.00	0.00	10972.93	B_1/A_2	0.00	0.07
$\widetilde{X}\ ^2A''(0,0,1)$	1100.87	1097.2	A_2/B_1	0.00	0.00	8626.76	B_1/A_2	0.00	0.06	11046.66	B_1/A_2	0.00	0.01
$\widetilde{X}\ ^2A''(0,1,0)$	1400.14	1391.5	A_2/B_1	0.00	0.00	8732.55	B_1/A_2	0.00	0.00	11164.30	A_2/B_1	0.00	0.04
$\widetilde{X}\ ^2A''(0,0,2)$	2181.55	2178.9	A_2/B_1	0.00	0.00	8852.90	B_1/A_2	0.00	0.17	11203.87	B_1/A_2	0.00	0.01
$\widetilde{X}\ ^2A''(0,1,1)$	2494.16	2472.6	A_2/B_1	0.00	0.00	8870.75	A_1/B_2	1.00	0.00	11219.37	B_1/A_2	0.00	0.40
$\widetilde{X}\ ^2A''(0,2,0)$	2781.64	2747.1	B_1/A_2	0.00	0.00	8880.14	B_1/A_2	0.00	0.01	11239.90	A_1/B_2	1.00	0.03
$\widetilde{X}\ ^2A''(0,0,3)$	3241.47	3245.8	A_2/B_1	0.00	0.00	8896.05	B_1/A_2	0.00	0.27	11283.47	B_1/A_2	0.00	0.11
$\widetilde{X}\ ^2A''(1,0,0)$	3454.06	3435.8	B_1/A_2	0.00	0.00	8962.38	B_1/A_2	0.00	0.00	11372.86	B_1/A_2	0.00	0.03
$\widetilde{X}\ ^2A''(0,1,2)$	3567.88	3538.4	B_1/A_2	0.00	0.00	9064.50	B_1/A_2	0.00	0.01	11405.62	B_1/A_2	0.00	0.89
$\widetilde{X}\ ^2A''(0,2,1)$	3866.74	3812.1	B_1/A_2	0.00	0.00	9153.07	A_2/B_1	0.00	0.17	11446.80	B_1/A_2	0.00	0.14
$\widetilde{X}\ ^2A''(0,3,0)$	4144.02	4071.0	B_1/A_2	0.00	0.00	9161.26	A_1/B_2	1.00	0.00	11484.57	A_1/B_2	1.00	0.00
$\widetilde{X}\ ^2A''(0,0,4)$	4280.19	4298.4	A_2/B_1	0.00	0.00	9164.79	B_1/A_2	0.00	0.00	11524.73	B_1/A_2	0.00	2.36
$\widetilde{X}\ ^2A''(1,0,1)$	4550.58	4529.2	B_1/A_2	0.00	0.00	9188.57	B_1/A_2	0.00	0.10	11533.08	A_1/B_2	0.99	0.08
$\widetilde{X}\ ^2A''(0,1,3)$	4620.92	4589.6	B_1/A_2	0.00	0.00	9290.77	B_1/A_2	0.00	0.01	11534.18	B_1/A_2	0.07	0.18
$\widetilde{X}\ ^2A''(1,1,0)$	4832.88	4793.7	B_1/A_2	0.00	0.00	9369.67	B_1/A_2	0.00	0.02	11545.33	A_1/B_2	1.00	0.06
$\widetilde{X}\ ^2A''(0,2,2)$	4932.14	4862.4	B_1/A_2	0.00	0.00	9421.00	A_2/B_1	0.00	0.34	11588.86	B_1/A_2	0.00	0.28
$\widetilde{X}\ ^2A''(0,3,1)$	5217.84	5119.4	B_1/A_2	0.00	0.00	9450.87	A_1/B_2	1.00	0.01	11610.06	B_1/A_2	0.00	0.01
$\widetilde{X}\ ^2A''(0,0,5)$	5297.33	5338.0	A_2/B_1	0.00	0.00	9481.67	B_1/A_2	0.00	0.37	11647.42	B_1/A_2	0.00	0.00
$\widetilde{X}\ ^2A''(0,4,0)$	5487.64[b]	5366.4	A_2/B_1	0.00	0.01	9548.99	B_1/A_2	0.00	0.00	11676.36	A_2/B_1	0.00	0.05
$\widetilde{X}\ ^2A''(1,0,2)$	5623.71	5605.2	B_1/A_2	0.00	0.00	9591.50	B_1/A_2	0.00	0.04	11716.97[c]	A_2/B_1	0.00	6.13
$\widetilde{X}\ ^2A''(0,1,4)$	5655.11	5630.1	B_1/A_2	0.00	0.00	9653.26	B_1/A_2	0.00	0.10	11792.67	A_1/B_2	1.00	0.01
$\widetilde{X}\ ^2A''(1,1,1)$	5917.75	5864.1	B_1/A_2	0.00	0.00	9723.37	B_1/A_2	0.00	0.00	11810.81	A_1/B_2	1.00	0.06
$\widetilde{X}\ ^2A''(0,2,3)$	5978.17	5900.6	B_1/A_2	0.00	0.00	9758.75	A_1/B_2	1.00	0.00	11843.18	A_2/B_1	0.00	0.04
$\widetilde{X}\ ^2A''(1,2,0)$	6189.55	6113.2	B_1/A_2	0.00	0.01	9839.01	B_1/A_2	0.00	0.06	11846.93	A_1/B_2	0.98	0.24
	6273.43		B_1/A_2	0.00	0.00	9875.59	A_2/B_1	0.00	0.07	11851.09	A_2/B_1	0.00	0.19
	6292.59		A_2/B_1	0.00	0.00	9912.10	B_1/A_2	0.00	0.02	11887.02	A_2/B_1	0.00	0.55
	6547.87		B_1/A_2	0.00	0.01	9928.35	B_1/A_2	0.00	0.28	11955.90	A_2/B_1	0.00	0.08
	6652.36		B_1/A_2	0.00	0.00	9936.90	B_1/A_2	0.00	0.02	11965.00	B_1/A_2	0.00	0.54
	6688.92		B_1/A_2	0.00	0.00	10058.77	A_1/B_2	1.00	0.01	11994.79	A_2/B_1	0.00	1.78
	6713.07		B_1/A_2	0.00	0.00	10065.02	B_1/A_2	0.00	0.01	12005.62	A_2/B_1	0.00	0.05
	6813.84		B_1/A_2	0.00	0.04	10160.07	B_1/A_2	0.00	0.14	12030.54	B_1/A_2	0.00	0.18
	6972.82		B_1/A_2	0.00	0.00	10201.74	B_1/A_2	0.00	0.50	12059.02	B_1/A_2	0.00	0.00
	7011.34		B_1/A_2	0.00	0.00	10238.20	B_1/A_2	0.00	0.07	12103.42	A_1/B_2	1.00	0.03
$\widetilde{A}\ ^2A'(0,0,0)$	7033.68	7030.0	A_1/B_2	1.00	0.00	10256.92	B_1/A_2	0.00	0.00	12149.07	A_2/B_1	0.00	0.15
	7257.81		B_1/A_2	0.00	0.02	10267.79	B_1/A_2	0.00	0.05	12160.36	A_2/B_1	0.00	1.25
	7265.49		B_1/A_2	0.00	0.00	10355.55	A_1/B_2	1.00	0.02	12197.30	A_2/B_1	0.00	5.33
	7312.80		B_1/A_2	0.00	0.01	10379.80	B_1/A_2	0.00	0.03	12272.59	B_1/A_2	0.00	2.59
	7526.88		B_1/A_2	0.00	0.07	10437.21	B_1/A_2	0.00	1.92	12287.38	B_1/A_2	0.00	0.02
	7592.83		B_1/A_2	0.00	0.01	10518.16	B_1/A_2	0.00	0.00	12357.68	B_1/A_2	0.00	0.02
	7640.53		B_1/A_2	0.00	0.00	10538.33	B_1/A_2	0.00	0.41	12396.39	A_1/B_2	1.00	0.00
	7720.78		B_1/A_2	0.00	0.00	10583.05	B_1/A_2	0.00	0.12	12410.53	A_1/B_2	1.00	0.11
	7807.10		B_1/A_2	0.00	0.00	10611.04	A_1/B_2	1.00	0.01	12443.86	A_1/B_2	1.00	0.01
	7858.75		B_1/A_2	0.00	0.07	10626.12	A_1/B_2	1.00	0.00	12449.49	A_2/B_1	0.00	3.48
$\widetilde{A}\ ^2A'(0,0,1)$	7962.13	7958.3	A_1/B_2	1.00	0.00	10651.97	A_1/B_2	1.00	0.06	12455.44	B_1/A_2	0.00	0.21
	7983.67		B_1/A_2	0.00	0.00	10669.90	B_1/A_2	0.00	0.05	12484.57	A_2/B_1	0.00	0.07
	8044.20		B_1/A_2	0.00	0.00	10696.14	B_1/A_2	0.00	0.00	12507.63[d]	A_2/B_1	0.00	12.98
	8108.56		B_1/A_2	0.00	0.03	10709.92	B_1/A_2	0.00	2.44	12587.04	A_2/B_1	0.00	0.01
	8125.52		B_1/A_2	0.00	0.27	10850.80	B_1/A_2	0.00	0.59	12594.80	A_2/B_1	0.00	0.49
	8217.58		B_1/A_2	0.00	0.00	10858.31	B_1/A_2	0.00	0.09	12652.45	A_1/B_2	1.00	0.01
$\widetilde{A}\ ^2A'(0,1,0)$	8243.36		A_1/B_2	1.00	0.00	10883.12	B_1/A_2	0.00	0.22	12673.27	A_2/B_1	0.00	0.28
	8292.87		B_1/A_2	0.00	0.01	10934.14	B_1/A_2	0.00	0.31	12716.91	A_1/B_2	1.00	0.23
	8344.16		B_1/A_2	0.00	0.02	10935.07	A_1/B_2	0.96	0.02	12732.25	A_2/B_1	0.00	5.77
	8574.59		B_1/A_2	0.00	0.09	10949.18	B_1/A_2	0.00	0.15	12732.67	A_1/B_2	1.00	0.01

As the energy increases the tunnelling splittings also increase. The lowest state, for which $\Delta \neq 0$ when given with two decimal places, is the bending state $\widetilde{X}(0,4,0)$ with $P_+ = 0$, marked (b) in Table III. The probability density function of this state is shown in Fig. 3(b). Even though this state has a noticeable splitting, it has zero probability density near the top of the barrier to H-O-O $\leftrightarrow$ O-O-H tunneling (at $\tau = 90°$). Nevertheless, the presence of the 13450-cm^{-1} barrier in the $\widetilde{X}\ ^2A''$ state and of the second potential energy minimum, on the other side of the barrier, influences the energy spectrum already at an energy of about 5500 cm^{-1}.

At still higher energy, larger tunneling splittings occur for the states with high bending excitation. In Figs. 3(c) and 3(d) the states with the largest tunnelling splittings (marked (c) and (d), respectively, in Table III) are shown. These states have energies of 11716.97 and 12507.63 cm^{-1} and Δ-values of 6.13 and 12.98 cm^{-1}, respectively. Both states have $\Gamma_{\rm rve} = A_2$ and 100% contribution from the lower electronic state; the symmetry of their respective partner states is $\Gamma_{\rm rve} = B_1$. The state in Fig. 3(d) has an appreciable, non-zero probability density at the T-shaped geometry with $\tau = 90°$. Hence, in this state, and states at higher energy with high bending excitation, the molecule can convert rather freely between its two versions.

With the DR program, we have calculated, and can calculate, thousands of rovibronic energies and it is clearly impractical to list them here. In Fig. 4 we show a term value diagram for all states with $J \leqslant 9/2$ and term values in the interval 6000-16000 cm^{-1} above the rovibronic ground state. We plot the term values against the probability P_+ of finding the molecule in the $\widetilde{A}\ ^2A'$ state. We do not include states with term values below 6000 cm^{-1} since they all have $P_+ = 0$; below 6000 cm^{-1} there are no $\widetilde{A}\ ^2A'$ rovibronic basis states available for interaction with the $\widetilde{X}\ ^2A''$ states and so no noticeable Renner coupling occurs. At 7034 cm^{-1}, however, $\widetilde{A}\ ^2A'$ rovibronic states emerge and interaction becomes more likely.

If we had drawn a diagram analogous to Fig. 4 for a Renner molecule with two component electronic states that both have linear equilibrium structures, such as $\widetilde{A}\ ^2\Pi$ MgNC/MgCN described in Refs. 32–34, we can predict its appearance from the 'standard' Renner theory[11] (see also, for example, Ref. 41 and references therein). This theory uses as zero order model two identical bending potential energy functions. That is, in the zero order model the electronic energy is doubly degenerate at all nuclear geometries, and the splitting into two non-degenerate states is treated as a perturbation. It is obvious that all vibronic states that

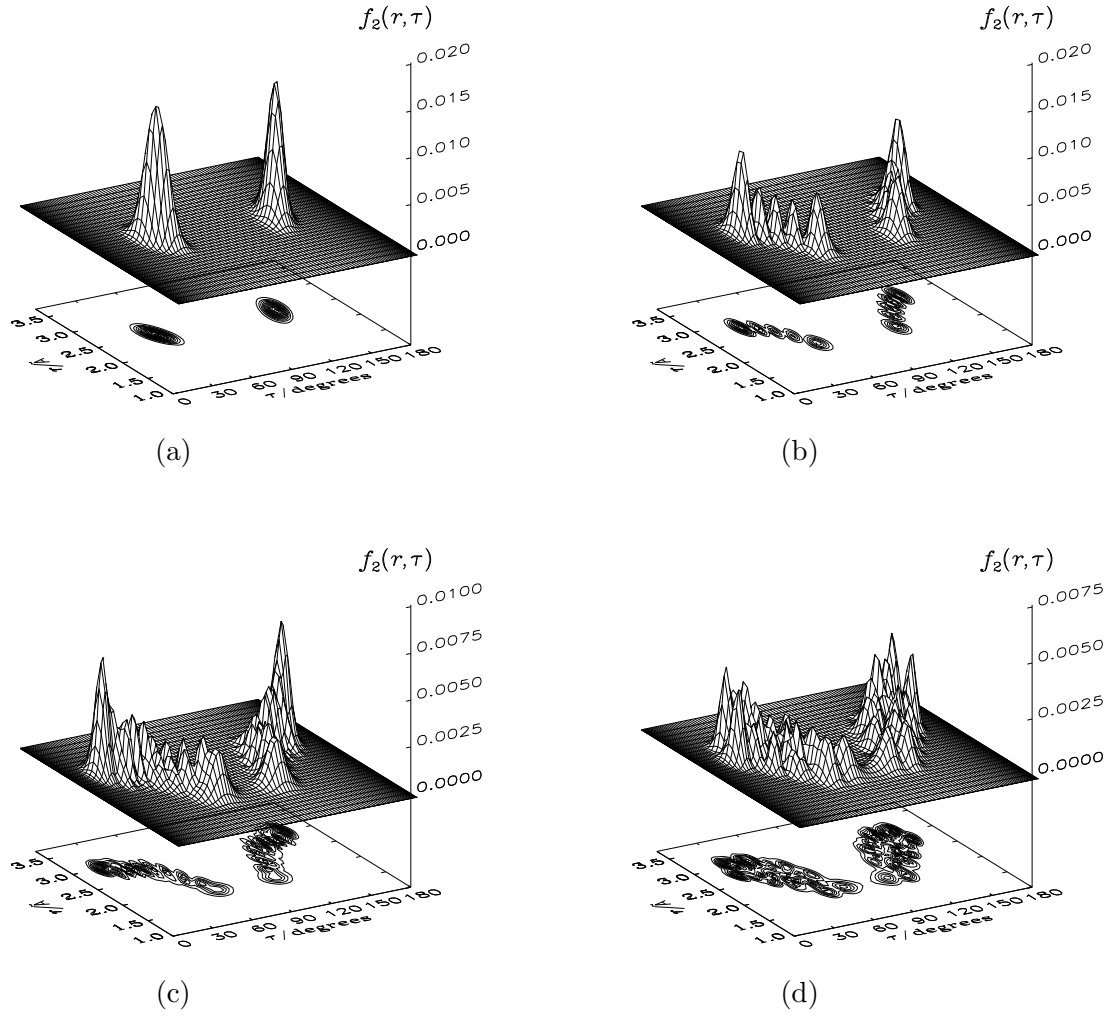

FIG. 3: Probability density functions $f_2(r,\tau)$ (see text) for the selected rovibronic states of HO_2 indicated in Table III.

suffer a first-order Renner interaction will have $P_+ \approx P_- \approx 0.5$, while there will be 'unique' levels, which have no near-by partner level to interact with, that will have $P_+ \approx 0$ or $P_+ \approx 1$. Thus, for a 'linear-linear' Renner molecule, we expect three vertical 'stripes' of levels with $P_+ \approx 0$, 0.5, and 1, respectively. Figure 4 shows that for HO_2, the situation is very different from the linear-linear case. For this bent-bent molecule, the Renner interactions are rather accidental and, in the region above 9000 cm^{-1} where the density of $\widetilde{X}\ ^2A''$ and $\widetilde{A}\ ^2A'$ states become high, basically all values of P_+ are represented.

In Fig. 4 we marked two states as (a) and (b), which represent a textbook example of an accidental resonance. The states have $J = 9/2$ and $N = K_a = 5$. Each of the two dots

in Fig. 4 represents four near-degenerate states. These four states comprise two state pairs originating in H-O-O $\leftrightarrow$ O-O-H tunneling. The one pair of states has $N_{K_aK_c} = 5_{50}$, and the other has $N_{K_aK_c} = 5_{51}$. For the (a) and (b) states with $N_{K_aK_c} = 5_{50}$, $\Gamma_{\rm rve} = A_2$, and term values of 7541.24 and 7541.67 cm^{-1}, respectively, we show the probability density functions $f_1(\tau)$ in Fig. 5. Symmetry requires that for all states, $f_1(\tau) = f_1(\pi - \tau)$. It can be recognized in Fig. 5 that the two states (a) and (b) result from an accidental resonance between, on the one hand, an $\widetilde{X}\ ^2A''$ basis state with two quanta of bending excitation (since the $f_-(\tau)$ function suggests a large contribution from a basis function with two nodes) and, on the other hand, an $\widetilde{A}\ ^2A'$ basis function with the no bending excitation, presumably the $K_a = 5$ level of $\widetilde{A}(0,0,0)$. The mixed states have 'symmetrical' values of (P_-, P_+) of (0.77,0.23) and (0.24,0.76), respectively.

V. SUMMARY AND DISCUSSION

In the present paper we report a theoretical investigation of the double Renner effect in the $\widetilde{X}\ ^2A''$ and $\widetilde{A}\ ^2A'$ electronic states of the HO_2 molecule. Three-dimensional potential energy surfaces have been calculated *ab initio* for these states with the core-valence MR-SDCI+Q/[cc-pVQZ (H), aug-cc-pCVQZ (O)] method. Global potential energy surfaces have been constructed by fitting analytical, parameterized functions through the *ab initio* data. These surfaces have been used for calculating HO_2 rovibronic energies in the 'double-Renner'-degenerate electronic state.

The calculated rovibronic energies and corresponding wavefunctions have been analyzed to investigate the influence of the H-O-O $\leftrightarrow$ O-O-H tunneling and the Renner interaction on the rovibronic energy spectrum. It was found that the effects of the H-O-O $\leftrightarrow$ O-O-H tunneling are significant at energies as low as 5500 cm^{-1}, almost 7950 cm^{-1} below the barrier to H-O-O $\leftrightarrow$ O-O-H tunneling in the ground electronic state. Also, we have demonstrated the accidental nature of the Renner interaction in a bent-bent molecule such as HO_2 [Figs. 4 and 5]. The accurate description of the Renner interaction for such molecules requires detailed numerical calculation by means of programs like RENNER[24–26] and DR;[32–34] it cannot be made by perturbation-theory models such as those used for linear-linear molecules.[11,41]

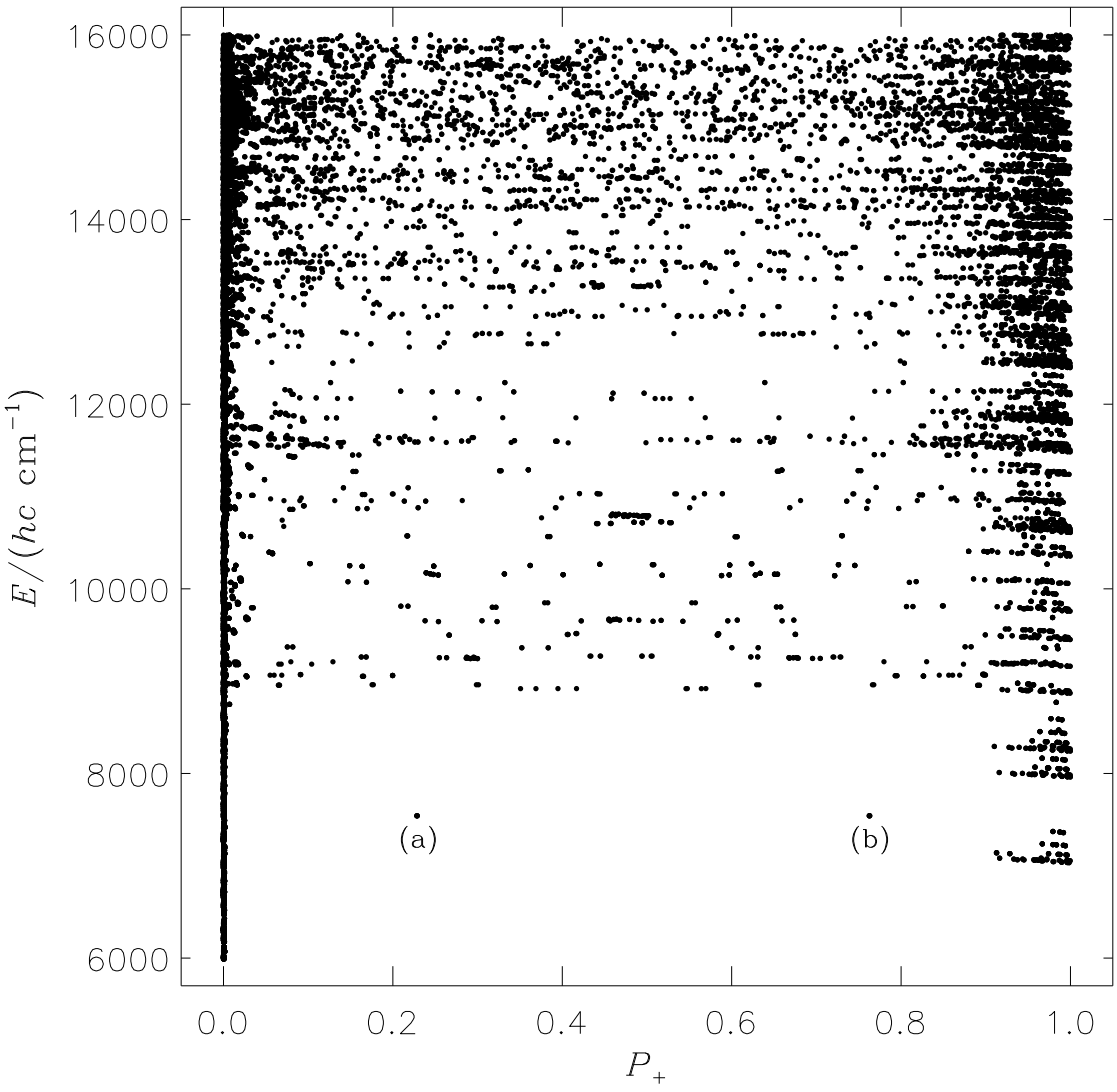

FIG. 4: Term value diagram for $\widetilde{X}\ ^2A''$ and $\widetilde{A}\ ^2A'$ HO_2. The energies are plotted against P_+, the contribution from the $\widetilde{A}\ ^2A'$ electronic state (see text).

Acknowledgments

Support from the European Commission through contract no. MRTN-CT-2004-512202 "Quantitative Spectroscopy for Atmospheric and Astrophysical Research" (QUASAAR) is acknowledged. The work of V. V. M., T. E. O., and P. J. was supported by the Deutsche Forschungsgemeinschaft and the Fonds der Chemischen Industrie. V. V. M. acknowledges

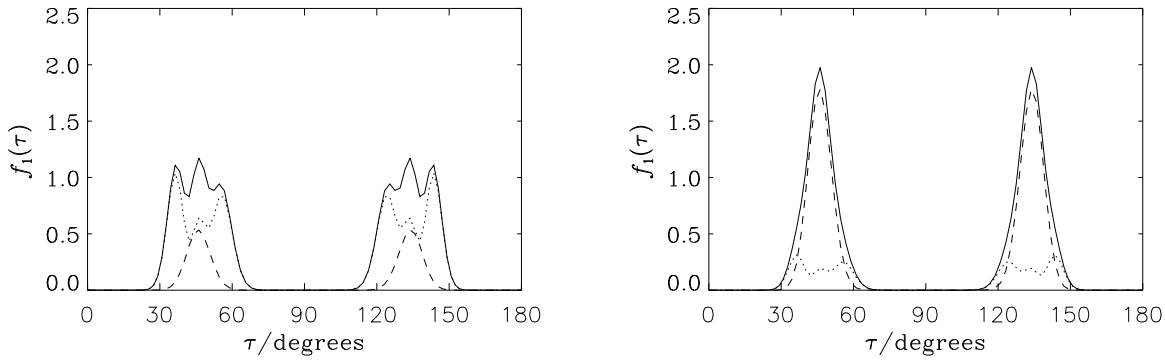

FIG. 5: Probability density functions $f_1(\tau)$, $f_-(\tau)$, and $f_+(\tau)$ (see text) for the selected rovibronic states of HO_2 indicated as (a) and (b) in Fig. 4. The solid curves represent $f_1(\tau)$, the dotted curves $f_-(\tau)$ (the $\widetilde{X}\ ^2A''$ state), and the dashed curves $f_+(\tau)$ (the $\widetilde{A}\ ^2A'$ state).

support from the Russian Federation President grant no. MK-8998.2006.8.

---

* Permanent address: Applied Physics Department, Tomsk Polytechnic University, Tomsk, 634050 Russia.

† Present address: Domaines Oceaniques, CNRS-UMR 6538, Institut Universitaire Européen de la Mer, Technopole Brest-Iroise, Place Nicolas Copernic, F-29280 Plouzane, France.

‡ Corresponding author. Tel: +49 202 439 2468. Fax: +49 202 439 2509. E-mail: jensen@uni-wuppertal.de

§ Present address: Research Institute for Computational Sciences, National Institute of Advanced Industrial Science and Technology, 1-1-1 Umezono, Tsukuba, Ibaraki 305-8568, Japan; E-mail: hirano@nccsk.com

[1] R. Zhu and M. C. Lin, PhysChemComm **23**, 1 (2001).

[2] M. E. Jenkin, Proc. EUROTRAC Symp. 98: Transp. Chem. Transform. Troposphere, ed. P. M. Borrell and P. Borrell, WIT Press, Southampton, 1999.

[3] A. Roger, Atmos. Environ. **34**, 2063 (2000).

[4] S. Viti, E. Roueff, T. W. Hartquist, G. Pineau des Foriêts, and D. A. Williams, Astron. Astro-

phys **370**, 557 (2001).

[5] L. B. Harding, J. Troe and V. G. Ushakov, Phys. Chem. Chem. Phys. **2**, 631 (2000).

[6] L. B. Harding, A. I. Maergoiz, J. Troe and V. G. Ushakov, J. Chem. Phys. **113**, 11019 (2000).

[7] J. Troe and V. G. Ushakov, J. Chem. Phys. **115**, 3621 (2001).

[8] A. D. Walsh, J. Chem. Soc. (Resumed), 2288 (1953).

[9] J. L. Gole and D. F. Hayes, J. Chem. Phys. **57**, 360 (1972).

[10] R. J. Buenker and S. D. Peyerimhoff, Chem. Phys. **28**, 299 (1978).

[11] R. Renner, Z. Physik **92**, 172 (1934).

[12] P. R. Bunker and P. Jensen, *Molecular Symmetry and Spectroscopy*, 2nd ed. NRC Research Press, Ottawa, 1998.

[13] P. Jensen, G. Osmann, and P. R. Bunker, *in: Computational Molecular Spectroscopy,* (P. Jensen and P. R. Bunker, eds.), Wiley, Chichester, 2000. See *http://www.chem.uni-wuppertal.de/cms/*

[14] H. E. Hunziker and H. R. Wendt, J. Chem. Phys. **60**, 4622 (1974).

[15] K. H. Becker, E. H. Fink, A. Leiss and U. Schurath, J. Chem. Phys. **60**, 4623 (1974).

[16] R. P. Tuckett, P. A. Freedman and W. J. Jones, Mol. Phys. **37**, 379 (1979).

[17] S. Saito and C. Matsumura, J. Mol. Spectrosc. **80**, 34 (1980).

[18] C. Yamada, Y. Endo, and E. Hirota, J. Chem. Phys. **78**, 4379 (1983).

[19] J. B. Burkholder, P. D. Hammer, C. J. Howard, J. P. Towle, and J. M. Brown, J. Mol. Spectrosc. **151**, 493 (1992).

[20] K. V. Chance, K. Park, K. M. Evenson, L. R. Zink, and F. Stroh, J. Mol. Spectrosc. **172**, 407 (1995).

[21] K. V. Chance, K. Park, K. M. Evenson, L. R. Zink, F. Stroh, E. H. Fink, and D. A. Ramsay, J. Mol. Spectrosc. **183**, 418 (1997).

[22] E. H. Fink and D. A. Ramsay, J. Mol. Spectrosc. **185**, 304 (1997).

[23] G. Osmann, P. R. Bunker, P. Jensen, R. J. Buenker, J.-P. Gu, and G. Hirsch, J. Mol. Spectrosc. **197**, 262 (1999).

[24] P. Jensen, M. Brumm, W. P. Kraemer and P. R. Bunker, J. Mol. Spectrosc. **171**, 31 (1995).

[25] M. Kolbuszewski, P. R. Bunker, P. Jensen and W. P. Kraemer, Mol. Phys. **88**, 105 (1996).

[26] G. Osmann, P. R. Bunker, P. Jensen and W. P. Kraemer, Chem. Phys. **225**, 33 (1997).

[27] P. Jensen, R. J. Buenker, J.-P. Gu, G. Osmann and P. R. Bunker, Can. J. Phys, **79**, 641 (2001).

[28] E. H. Fink and D. A. Ramsay, J. Mol. Structure **795**, 155 (2006).

[29] J. D. DeSain, A. D. Ho, and C. A. Taatjes, J. Mol. Spectrosc. **219**, 163 (2003).

[30] P. R. Bunker and P. Jensen, *in: Computational Molecular Spectroscopy,* (P. Jensen and P. R. Bunker, eds.), Wiley, Chichester, 2000. See *http://www.chem.uni-wuppertal.de/cms/*

[31] R. G. A. Bone, T. W. Rowlands, N. C. Handy and A. J. Stone, Mol. Phys. **72**, 33 (1991).

[32] T. E. Odaka, *The Double Renner Effect*. Ph.D. dissertation, University of Wuppertal, Germany, and Ochanomizu University, Tokyo, Japan, 2003. See EPAPS Document No. E-JCPSA6-126-002708 for a pdf file with the Ph.D. thesis. This document can be reached via the EPAPS homepage http://www.aip.org/pubservs/epaps.html.

[33] T. E. Odaka, T. Hirano, and P. Jensen, J. Mol. Structure **795**, 14 (2006).

[34] T. E. Odaka, V. V. Melnikov, P. Jensen, T. Hirano, B. Lang and P. Langer, J. Chem. Phys. **126**, 094301 (2007).

[35] E. Anderson, Z. Bai, C. Bischof, S. Blackford, J. Demmel, J. Dongarra, J. Du Croz, A. Greenbaum, S. Hammarling, A. McKenney, and D. Sorensen, *LAPACK Users' Guide*, 3rd ed., SIAM, Philadelphia, PA, 1999.

[36] MOLPRO, a package of ab initio programs designed by H.-J.Werner and P. J. Knowles, version 2002.6, R. D. Amos, A. Bernhardsson, A. Berning, P. Celani, D. L. Cooper, M. J. O. Deegan, A. J. Dobbyn, F. Eckert, C. Hampel, G. Hetzer, P. J. Knowles, T. Korona, R. Lindh, A.W. Lloyd, S. J. McNicholas, F. R. Manby, W. Meyer, M. E. Mura, A. Nicklass, P. Palmieri, R. Pitzer, G. Rauhut, M. Schütz, U. Schumann, H. Stoll, A. J. Stone, R. Tarroni, T. Thorsteinsson, and H.-J. Werner.

[37] T.H. Dunning, Jr., J. Chem. Phys. **90**, 1007 (1989).

[38] D. E. Woon and T. H. Dunning, Jr., J. Chem. Phys. **103**, 4572 (1995).

[39] R. A. Kendall, T. H. Dunning, Jr., and R. J. Harrison, J. Chem. Phys. **96**, 6769 (1992).

[40] S. R. Langhoff and E. R. Davidson, Int. J. Quantum Chem. **8**, 61 (1974).

[41] J. M. Brown, *in: Computational Molecular Spectroscopy,* (P. Jensen and P. R. Bunker, eds.),

Wiley, Chichester, 2000. See *http://www.chem.uni-wuppertal.de/cms/*

FIGURE CAPTIONS

Fig. 1 The Jacobi coordinates, and the molecule-fixed axis system xyz, for HO_2. The O nuclei are labeled 1 and 2, respectively, as indicated, and the proton is labeled 3. M is the center of mass of the OO moiety. The O-O internuclear distance is called R, r is the M-H distance, and $\tau = \angle(O_1\text{-M-H})$ where O_1 is the oxygen nucleus labeled 1. The xyz axis system has origin in the nuclear center of mass. The z axis is parallel to the O-O bond, and the x axis points into the plane of the page so that the xyz axis system is right-handed.

Fig. 2 The bending minimum energy paths for HO_2. The solid curve corresponds to the $\widetilde{X}\ ^2A''$ electronic state and the dashed curve to the $\widetilde{A}\ ^2A'$ state.

Fig. 3 Probability density functions $f_2(r,\tau)$ (see text) for the selected rovibronic states of HO_2 indicated in Table III.

Fig. 4 Term value diagram for $\widetilde{X}\ ^2A''$ and $\widetilde{A}\ ^2A'$ HO_2. The energies are plotted against P_+, the contribution from the $\widetilde{A}\ ^2A'$ electronic state (see text).

Fig. 5 Probability density functions $f_1(\tau)$, $f_-(\tau)$, and $f_+(\tau)$ (see text) for the selected rovibronic states of HO_2 indicated as (a) and (b) in Fig. 4. The solid curves represent $f_1(\tau)$, the dotted curves $f_-(\tau)$ (the $\widetilde{X}\ ^2A''$ state), and the dashed curves $f_+(\tau)$ (the $\widetilde{A}\ ^2A'$ state).

Fig. 1

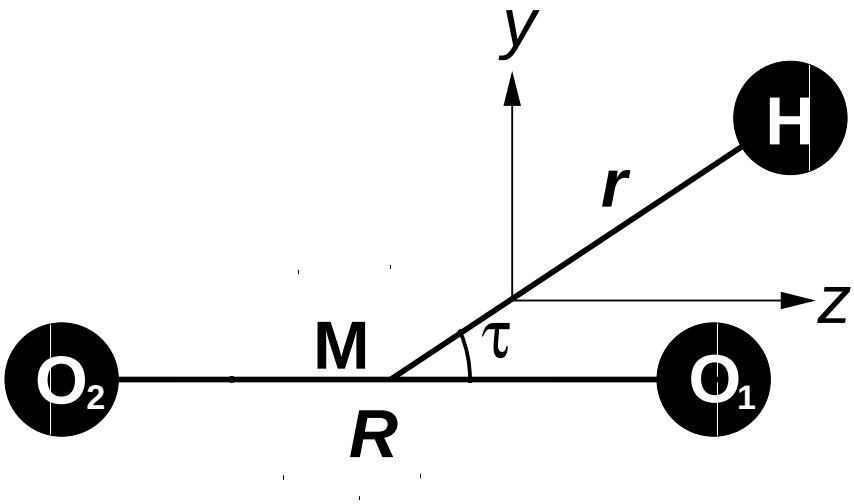

Fig. 2

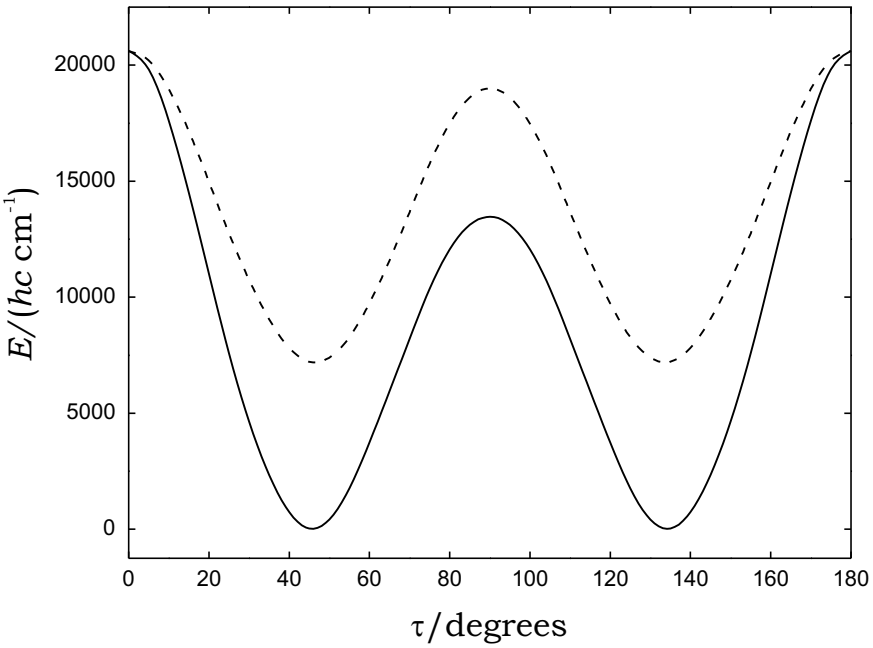
20000
15000
10000
5000
0
0
20
40
60
80
100
120
140
160
180
E/(hc cm-1)
τ/degrees

Fig. 3

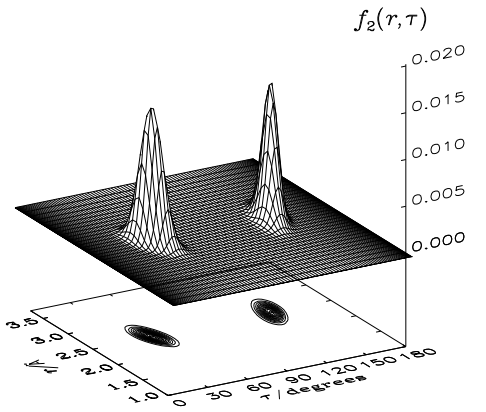
$f_2(r,\tau)$
0.020
0.015
0.010
0.005
0.000
3.5
3.0
2.5
2.0
1.5
1.0
r
0
30
60
90
120
150
180
τ / degrees

(a)

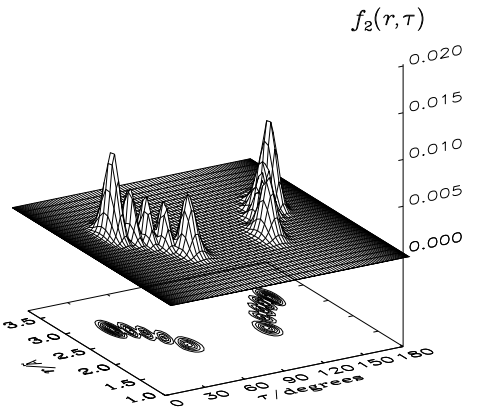
$f_2(r,\tau)$
0.020
0.015
0.010
0.005
0.000
3.5
3.0
2.5
2.0
1.5
1.0
r
0
30
60
90
120
150
180
τ / degrees

(b)

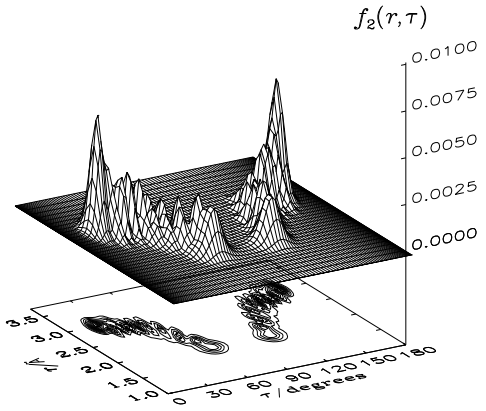
$f_2(r,\tau)$
0.0100
0.0075
0.0050
0.0025
0.0000
3.5
3.0
2.5
2.0
1.5
1.0
r
0
30
60
90
120
150
180
τ / degrees

(c)

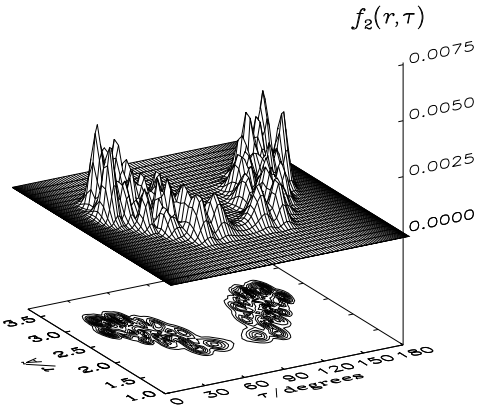
$f_2(r,\tau)$
0.0075
0.0050
0.0025
0.0000
3.5
3.0
2.5
2.0
1.5
1.0
r
0
30
60
90
120
150
180
τ / degrees

(d)

Fig. 4

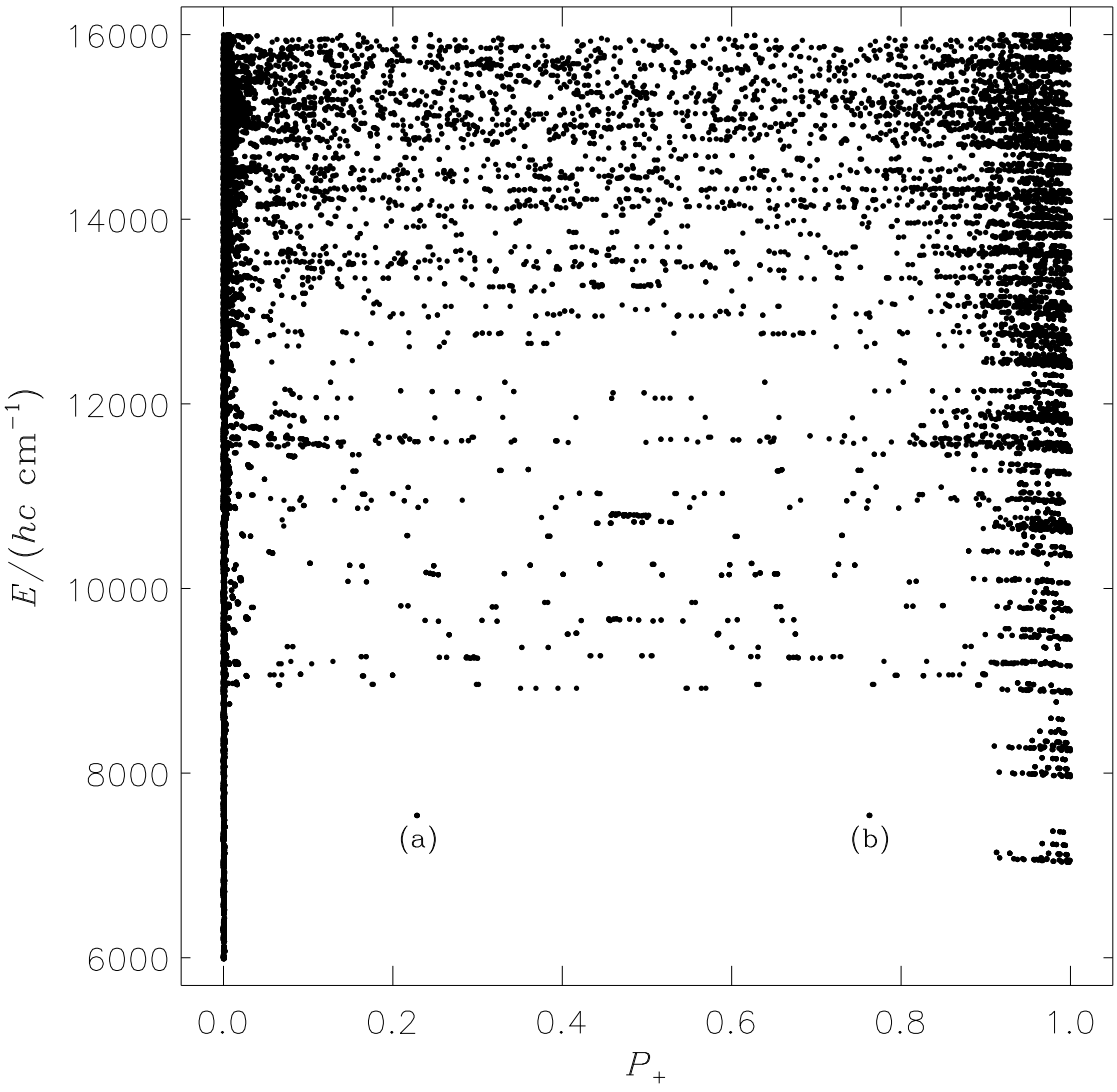
16000
14000
12000
10000
8000
6000
$E/(hc\ \mathrm{cm}^{-1})$
0.0
0.2
0.4
0.6
0.8
1.0
P_+
(a)
(b)

Fig. 5

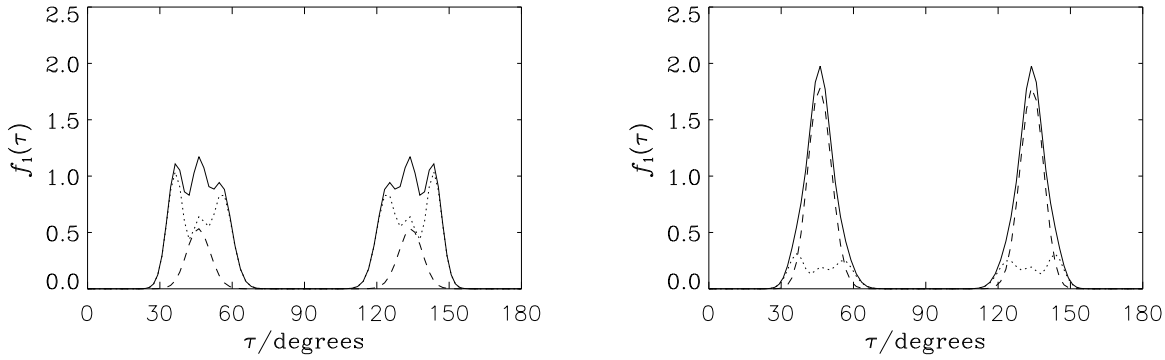
2.5
2.0
1.5
1.0
0.5
0.0
$f_1(\tau)$
0
30
60
90
120
150
180
τ/degrees
(a)
2.5
2.0
1.5
1.0
0.5
0.0
$f_1(\tau)$
0
30
60
90
120
150
180
τ/degrees
(b)